EXAMINATION OF DYNAMIC CHARACTERISTICS OF A CONEX CONTAINER IN DUAL POINT CARRIAGE FROM SIMULATION AND WIND TUNNEL TEST

Zhouzhou Chen, Joseph F. Horn, and Jacob Enciu, The Pennsylvania State University, State College PA, USA

Reuben Raz and Aviv Rosen, Technion-Israel Institute of Technology, Haifa, Israel

Luigi Cicolani, San Jose State Research Foundation, Moffet Field CA, USA

Abstract

This paper discusses the observations and results from wind tunnel tests and simulations of an isolated 6x6x8 ft CONEX cargo container carried in a 2-point inverted-V suspension with a laterally active forward cargo hook (ACH). Wind tunnel tests on a model-scale configuration showed a growing roll-yaw limit cycle oscillation in forward flight with a progressive shifting of the load from the rear hook to the forward hook as the speed increased and eventual rear cable slackening. A simulation model of the full-scale load-suspension configuration was developed and achieved good agreement with the wind tunnel results after including the nonlinear stretching properties of the test cables and accounting for the unsteady aerodynamics of the CONEX. A lateral ACH controller design based on the linearized simulation model showed good load stabilization performance using lagged load attitude feedback. Load distribution to the two hooks could be controlled by cable length adjustments at the rear hook.

1. NOTATION

Acronyms

ACH Active Cargo Hook

CFD Computational Fluid Dynamics

CONEX Container and Express

HMMWV High Mobility Multipurpose Wheeled Vehicle

LCO Limit Cycle Oscillation

MILVAN Military-Owned Demountable Container

Symbols

β Side-slip angle, deg

ω Natural frequency, rad/s

ϕ_L, θ_L, ψ_L Load Euler angles, deg

τ Time constant, sec

τ_F, τ_R Forward and rear hook force magnitudes, g

θ_F, ϕ_F Forward hook force direction angles, deg

θ_R, ϕ_R Rear hook force direction angles, deg

ζ Damping ratio

C_N Nondimensional yaw moment coefficient

Gm, Pm Gain and phase margin, dB, deg

K ACH controller gain, ft/rad

K_P, K_I Proportional and integral gain

p_L, q_L, r_L Load Euler angle rates, deg/s

u_L, v_L, w_L Load velocities, ft/s

x_E, y_E, z_E Load position in inertial coordinate, ft

Y_{cmd} Forward cargo hook command position, ft

2. INTRODUCTION

Dual-point suspensions received substantial attention in the 1960s and 1970s in connection with the heavy lift Helicopter project intended to carry military loads exceeding 20000 lbs. Difficult loads such as the 20x8x8 ft MILVAN cargo container was known to be unstable at low forward speeds when carried in a single-point suspension, commonly due to yaw-lateral instabilities. The dual point suspension allows the load to be carried in a minimum drag orientation and provides yaw restraint to delay the onset of instability to higher speeds with the underlying aspiration of carrying difficult loads to the power-limited speeds of the helicopter-load configuration for purposes of supply efficiency and safety in combat zones. Since then, interest in dual point suspensions has been renewed in determining the safe speed envelope for slung loads carried by the V-22 rotorcraft which is capable of speeds exceeding 200 knots.

There are many dual-point references from the heavy lift design period conducted in the US by VERTOL and others and in the UK by the Royal Military College of Science (RMCS) and others. Gable and Wilson conducted early research on the instability of slung loads using simulation, wind tunnel, and flight test data [1]. The work identified the principal instabilities to be related to sling elasticity (vertical bounce mode of the coupled helicopter and load) and load aerodynamic instability primarily in the lateral-directional degrees of freedom. It concluded that 2-point suspensions using longitudinally spaced hooks can restrain yaw and extend the speed onset of instability to well above 100 knots for the test loads. Later research on dual-point load instability includes ([2],[3],[4]). Reference [2] describes the types of instability observed in a comprehensive wind tunnel study of box-shaped loads, hook arrangements, and rigging geometries. In reference [3], simulations of a V22 carrying an HMMWV in tandem 2-point suspension were conducted. The simulation model predicted the correct pendulum modes but did not reproduce the yaw-lateral modes. An isolated HMMWV load model carried in inverted V suspension was studied in [4] and showed an unstable yaw limit cycle oscillation (LCO) that started at low airspeed (30 knots). They explained that the LCO was related to the height of the load center of gravity (c.g.) relative to the front lift points.

This paper discusses the observations and results from simulations and wind tunnel tests of an isolated 6x6x8 ft CONEX cargo container carried in an inverted V configuration with a laterally active forward cargo hook (ACH). It particularly addresses the importance of modeling the unsteady aerodynamic effects and sling elasticity in order to produce the observed dynamic characteristics of a dual-point suspended load. A simulation model of the load and suspension was initially developed using a linear spring model of cable elasticity and the load static aerodynamics. The preliminary simulation showed the expected pendulum modes and a damped roll-yaw mode in forward flight. Wind tunnel tests were conducted at the Technion-Israel Institute of Technology to verify the simulation. The test configuration consisted of a scaled load model, four nylon cables, and two longitudinally spaced cargo hooks. The test runs included airspeed sweeps and ACH frequency sweeps at selected airspeeds. The results showed that the roll-yaw mode was an unstable LCO at airspeeds where the simulation model predicted stable behavior. A stretching test of the cables revealed that the test cables had nonlinear elasticity and were significantly more elastic at lower tensions. Hysteresis was also present in the cable tension forces. A model of the CONEX unsteady yaw moment derived in [5] was later integrated into the simulation. After modifying the cable elasticity model and adding the unsteady aerodynamic effects of the box, the simulation matched the load LCO seen in the wind tunnel tests. After validating the simulation model, a preliminary control design was conducted based on the extracted linear model. The active stabilization using forward hook lateral motion is demonstrated with the designed linear controller and the simulation.

In the following sections, the paper discusses the wind tunnel tests, the simulation development and validation, linear analysis, and the design of the controller and results.

3. WIND TUNNEL TEST

The wind tunnel tests were carried out at the Technion-Israel Institute of Technology low-speed wind tunnel with 1x1m cross-section. The configuration was scaled 11:1, with two weights corresponding to the empty container (2400lbs full-scale referred to as the 2K CONEX) and a ballasted weight (4400lbs full-scale, referred to as the 4K CONEX). Hook separation corresponded to the 160-inch hook separation of the CH47D and sling legs were scaled to those of the standard military sling set used to suspend the CONEX (16ft). All results in this paper will be given at full scale. Froude scaling was used to convert between model-scale and full-scale dynamics and airspeed. The scaling rules can be found in [6] as it also showed that Froude scaling accurately predicts the full-scale dynamics from the model scale wind tunnel data. The reason for the accuracy of Froude-scaled dynamics is that the aerodynamic coefficients are independent of Reynolds number for most bluff bodies like the CONEX, and thus are the same at any scale. The tests included two phases: During the first phase both hooks were fixed in each test. The second phase included a forward hook capable of controlled lateral motion and a fixed rear hook.

Figure 1: Wind tunnel test set-up (first phase)

3.1. The first phase of the test

The purpose of the first phase was to perform an initial study of the load dynamics in the case of dual point suspension and to check the agreement between the test results and the initial results of a preliminary simulation model. Such comparisons helped in tuning the model, identifying problems of the simulation, and suggesting changes and refinements of the simulation to improve the agreement. Figure 1 shows a model in the wind tunnel during the first phase. A small instrumentation package in the CONEX model measured accelerations, angular rates, and Euler angles. An airspeed sweep from 2-16 m/s (15-105 knots full-scale) was conducted to reveal the dynamics of the load over the speed envelope.

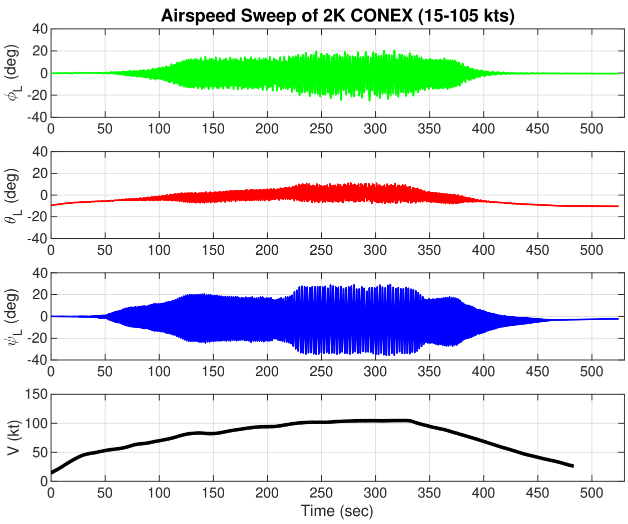

Figure 2: Airspeed sweep of 2K CONEX from 15-105 knot

Figure 2 shows the time history plot of the load attitude angles and the wind tunnel airspeed at full-scale. Load oscillation started to develop at 50 knots and the amplitude gradually increased with airspeed until 80 knots, where the load settled into an LCO of 20° in yaw and 15° in roll. The amplitude of the LCO increased at 100 knots on all axes ($\psi_L = \pm 27°, \phi_L = \pm 20°, \theta_L = \pm 8°$). The LCO was catastrophic at 16 m/s (104 kt full-scale) when the rear cable became slack, and the test was immediately stopped to avoid damage to the equipment. From the initial airspeed sweep result, differences from the preliminary simulation model were noticed such that the local stability of the load predicted by the model disagreed with the airspeed sweep result. These observations led to changes in the simulation model, which will be discussed in later sections. In addition to the 2K load configuration, similar airspeed sweeps were conducted on several other configurations including a heavier 4K load model as shown in figure 3, and it shows that by increasing the weight, it was possible to reach higher speeds before encountering severe LCO.

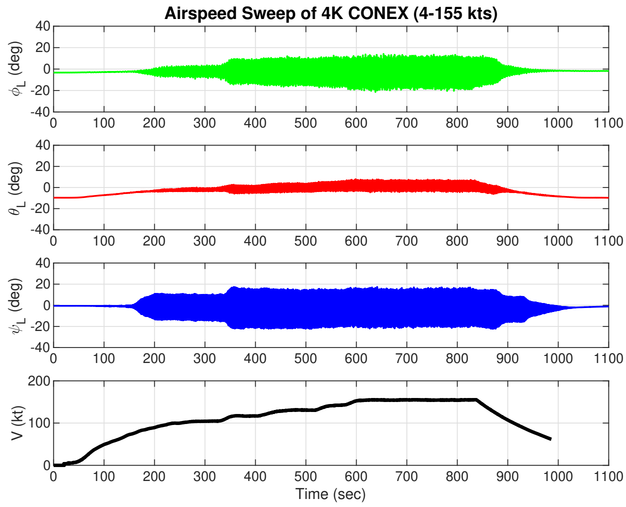

Figure 3: Airspeed sweep of 4K CONEX from 4-155 knot

3.2. The second phase of the test

For the second phase of the test, an active cargo hook set-up was implemented as shown in figure 4. A frame made of standard extruded aluminum was attached to the tunnel ceiling. Rollers that slide on the frame allowed for the lateral motion of the forward hook which was commanded by an electric step motor with a toothed pulley and timing belt. An IR sensor was used to measure the lateral position of the forward hook. The rear hook was rigidly attached to the back of the frame. In all the tests the rear hook was higher by 60 mm (26-inch full-scale) relative to the forward hook, representing typical flight conditions of a rotorcraft pitching down. The hooks included load cells and gimbals to measure the magnitudes and direction angles of the forces applied to the hooks by the cables. Cable lengths were adjusted for the gimbal and load cell so that the distance from the hook to lift points on the load remained at 16ft full-scale.

Figure 4: Wind tunnel test set-up (second phase)

The test matrix included lateral frequency sweeps of the forward hook with different amplitudes at selected airspeeds. The frequency sweeps were used to identify linear models of the load dynamics. For the 2K weight model, 15 frequency sweeps were performed in the speed range from 15 to 105 knots. For the 4K weight 9 frequency sweeps were performed in the speed range from 15 to 156 knots. Figure 5 shows an example frequency sweep of the 2K CONEX at 78 knots. Figure 5(a) shows the sweep input and the closed-loop control action of the forward lateral hook and the time response of the load attitudes in all three axes. Figure 5(b) shows the hook force direction angles and the hook force magnitudes measured from the two hooks. The time history plots show that the load was unstable at the speed and displayed LCO motion primarily in the lateral axis. The test also implemented an ACH controller from a previous single-point suspension study that used hook force direction angles feedback for load stabilization [7]. The controller was turned on at 360 seconds and, as seen in figure 5, it succeeded in suppressing the LCO in all variables. This was an early indication that the ACH would be able to stabilize the LCO. However, the unoptimized controller lost its effectiveness at the highest test speed.

3.3. Steady-state behavior and LCO analysis

The second phase tests allowed time for the load amplitude to develop to its steady-state value at each

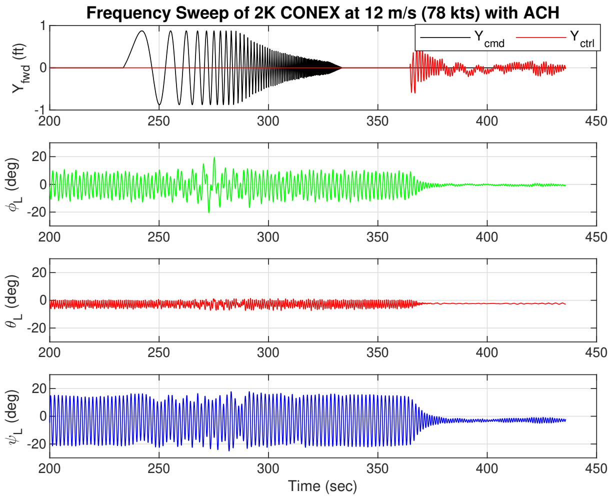

(a) Hook position and load attitude angles

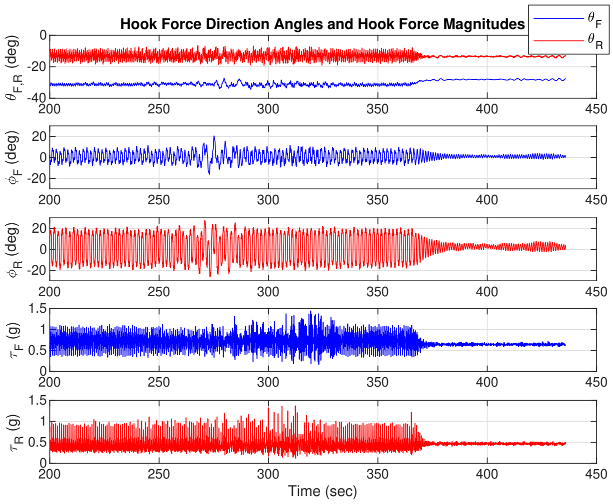

(b) Hook direction angles and hook force magnitudes

Figure 5: Frequency sweep of 2K CONEX at 78 knots with Active Cargo Hook (ACH)

airspeed and were used for the study of the load behavior during forward flight. Figure 6 shows the trim/steady-state values of the load at the tested airspeeds marked by the triangle shape. In hover the load was stable and there was a steady trim in all variables. In forward flight there was a steady state LCO and 'trim' was defined by the mean values of the undamped oscillations. The first plot shows the forward and rear hook forces (τ_F,τ_R), and as airspeed increased, the load shifted toward the forward hook as the load c.g. shifted rearward due to increasing load drag. The hook force direction angles in the second plot show the change in pitch angle of the front and rear (θ_F,θ_R) inverted V triangles was about 30 degrees, corresponding to the rear movement of the load c.g. position. Steady-state yaw/sideslip ψ_L and roll ϕ_L shown in plot 4 were at near zero as expected for the dual point suspension. This was consistent with the near-zero steady-state values of ϕ_F, ϕ_R shown in plot 3.

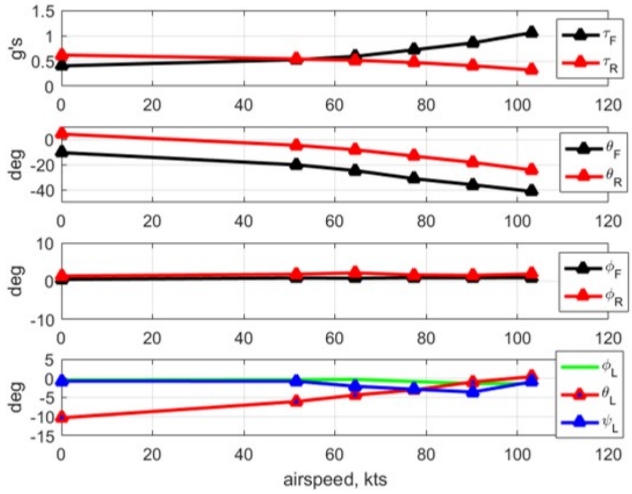

Figure 6: Steady state behavior of the load

Figure 7 shows 5 seconds of LCO from the start of the sweep in figure 5 prior to any ACH input. From the first plot, we can see that the LCO in load roll and yaw attitude had the same frequency with 180° relative phase. In the second plot, small periodic θ_L at half the LCO period in the lateral axis was present. The hook force direction angles in plots 3 and 4 showed a similar trait of the longitudinal LCO having twice the frequency of the lateral LCO plus higher frequency oscillations. The last plot shows the hook force magnitudes varying at higher frequencies than the observed LCO due to the cable stretching modes. Figure 8 shows the amplitudes and frequency of the LCO in the Euler angles at all forward flight test speeds. The mode was dominated by yaw with increasing participation of roll. These oscillations grew with airspeed to levels of operational concern by 70-80 knots. It was visible in the time histories that yaw and roll oscillations occurred at the same frequency, and at 78 knots and above pitch was periodic at twice the yaw/roll frequency and seemed to be included in the LCO. The dashed blue line indicates the frequency of the yaw and roll oscillations in the LCO which had a range of 2.5 to 4.5 rad/sec.

3.4. Conclusion of the wind tunnel test

The wind tunnel test has revealed the important dynamic characteristics of the dual-point CONEX in both hover and forward flight conditions. In hover, the dominant dynamics of the load was a lightly-damped lateral pendulum, which damped out to a steady trim attitude with no LCO under excitation. In forward flight, a roll-yaw-coupled LCO was excited by any disturbance and dominated the steady-state load motion. The amplitude of the LCO increased with airspeed and eventually became chaotic. The closed-loop test verified the feasibility of load stabilization with an active forward lateral hook and showed that the LCO motion was damped out in all axes by the hook force angle feedback controller. Most importantly, the wind tunnel test showed discrepancies with the preliminary simulation model and prompted revisions on several aspects of the model, which will be discussed in the next section.

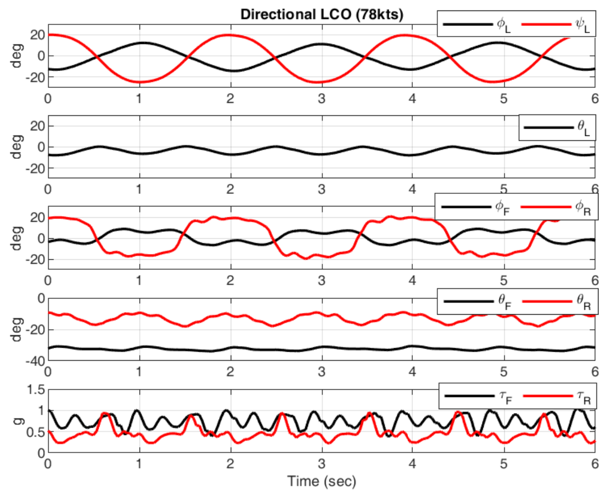

Figure 7: Directional LCO at 78 knots

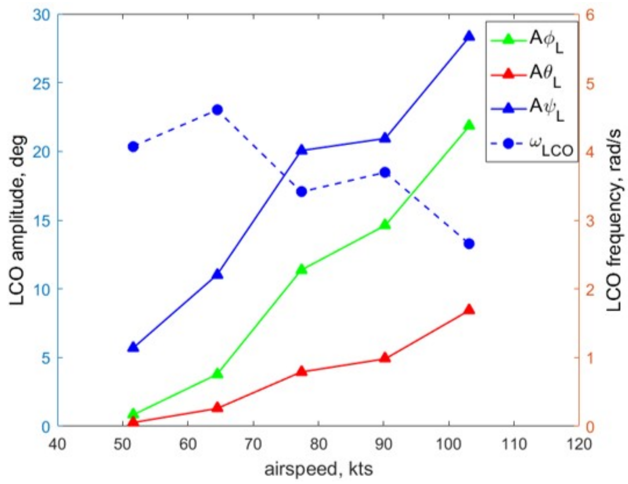

Figure 8: LCO amplitudes and frequency (Load Euler Angles)

4. SIMULATION MODEL AND LINEAR ANALYSIS

The development of the simulation model can be divided into two phases. During the first phase, an isolated load model was constructed in MATLAB/SIMULINK where the geometric and inertial properties of the load were defined. The simulation model adopted the mass and inertial properties of the

CONEX load measured in ref [6]. The hook geometry imitated a CH-47 Chinook with a spacing of 160 inches between the forward and rear cargo hooks. A conventional rigging procedure with four equal-length cables was applied with cable lengths equal to 16 ft. The suspension was modeled as a linear spring system with the cable elastic properties being set based on the data provided in [8]. The model used a validated static aerodynamic database [9] to reproduce the aerodynamic coefficients given the free-stream velocity, load orientation, and angular rates. The equations of motion for the system included the standard six degrees of freedom equations for a rigid body: 6 equations for the calculation of the linear and angular accelerations with three equations for the calculation of the accelerations of the load center of mass in the body axes (eq.1), and three equations for the calculation of load angular accelerations (eq.2).

(1) $$\vec{a}_L^b = \frac{\vec{F}_L^b}{m_L} - \vec{\omega}_L^b \times \vec{v}_L^b$$

(2) $$\vec{\alpha}_L^b = J^{-1} \cdot \{\vec{M}_L^b - [\vec{w}_L \times (J \cdot \omega_L^b)]\}$$

The twelve element state vector of the system, X_L, is given as:

(3) $$X_L = \{p_L, q_L, r_L, \psi_L, \theta_L, \phi_L, u_L, v_L, w_L, x_E, y_E, z_E\}$$

where p_L,q_L,r_L are the angular rates in a load fixed coordinates system (L), ψ_L,θ_L,ϕ_L are the standard 3-2-1 Euler angles, u_L,v_L,w_L are the inertial velocity components in the load fixed coordinate system. x_E,y_E,z_E are the components of the load center of mass vector, expressed in an inertial coordinate system (E) that is attached to the wind tunnel floor with the x-axis directed into the incoming flow and z-axis directed down. Figure 9 shows the two coordinate systems used and the rigging pattern from the cables.

4.1. Modifications of the preliminary simulation model

After the wind tunnel tests, it was noticed that the simulation results did not agree with the load dynamics observed from the tests. At speeds below 50 knots, the simulation model predicted an unstable lateral pendulum mode, while the wind tunnel showed stable load responses. At higher airspeed, the simulation model predicted stable load dynamics while the wind tunnel test showed unstable LCO motion. The mismatch between the simulation model and the wind tunnel test results signaled the insufficiency of the model

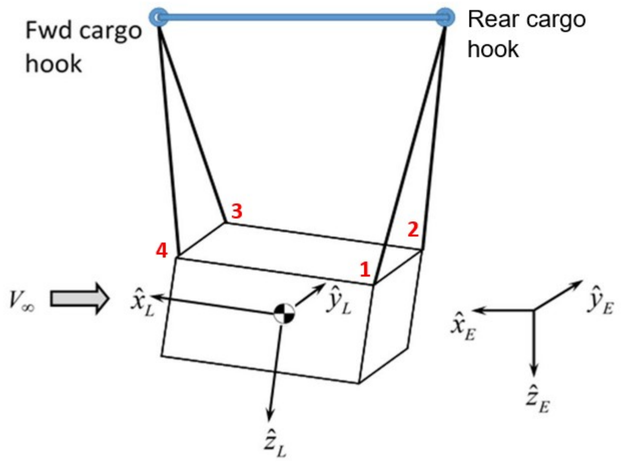

Figure 9: Load fixed (L) and wind tunnel inertial (E) coordinate systems (lift points labeled in red)

and thus required modifications. The dynamic inconsistencies between the two were suspected to be related to the aerodynamics and the suspension models. This led to the second phase of the simulation model development.

The preliminary simulation model used static aerodynamic data measured in the wind tunnel combined with quasi-steady derivatives to generate forces and moments. It was pointed out by multiple resources ([10],[11],[5]) that unsteady aerodynamic effects are present in bluff bodies, and static or quasi-static descriptions are insufficient to characterize their aerodynamics fully. Unsteady aerodynamics of bluff bodies are in general, a complicated flow phenomenon to model. It comprises the unsteady effects of the stationary container due to vortex shedding and of the oscillating container due to phase lags in separation bubble growth. From earlier wind tunnel tests ([10],[11]), it was discovered that subjecting bluff bodies to forced oscillations yielded frequency-dependent aerodynamic coefficients. In [5], a modeling method was proposed that captured the unsteady aerodynamic effects of the CONEX up to 130 knots. The method utilized computational fluid dynamics (CFD) and frequency domain identification methods to identify the aerodynamic coefficients from forced oscillations in side-slip angle. A second-order transfer function model was identified to represent the container's lateral-directional aerodynamics throughout the frequency range of the forced oscillation. The second-order transfer function has the form:

(4) $$\frac{CN(s)}{\Delta\beta(s)} = \frac{a_2 s^2 + a_1 s + a_0}{b_2 s^2 + b_1 s + 1}$$

The Δ term indicates the deviation from the trim value of the side-slip angle. In [5], $\beta_0 = 90°$ corresponded to

$a_2(sec^2/deg)$	$a_1(sec/deg)$	$a_0(deg^{-1})$
$-.9863e-4$	$-.3831e-3$	$.4322e-2$
$b_2(sec^2)$	$b_1(sec)$	b_0
$.01389$	$.1126$	1

Table 1: Coefficients of transfer function fits at V=60 knots (from [5])

the load orientation presented in this paper. The coefficients were identified at the reference speed of 60 knots. At other airspeeds, the time dependence varied such that derivatives with respect to dimensionless time ($t \cdot V/L$) were invariant. The simulation model valid at all airspeeds is shown in equation 5, where V_{ref} and V represent the reference airspeed of the identified coefficients and the actual speed. The coefficients a_0, a_1 are associated with static and quasi-static aerodynamics, and a_2, b_1, b_2 are associated with unsteady aerodynamic effects from higher-order angle derivatives and other terms. This model was implemented into the simulation model for calculating the yaw moment coefficient C_N at all airspeeds.

$$\frac{CN(s)}{\Delta\beta(s)} = \frac{(a_2 * \frac{V_{ref}}{V}^2)s^2 + (a_1 * \frac{V_{ref}}{V})s + a_0}{(b_2 * \frac{V_{ref}}{V}^2)s^2 + (b_1 * \frac{V_{ref}}{V})s + 1} \tag{5}$$

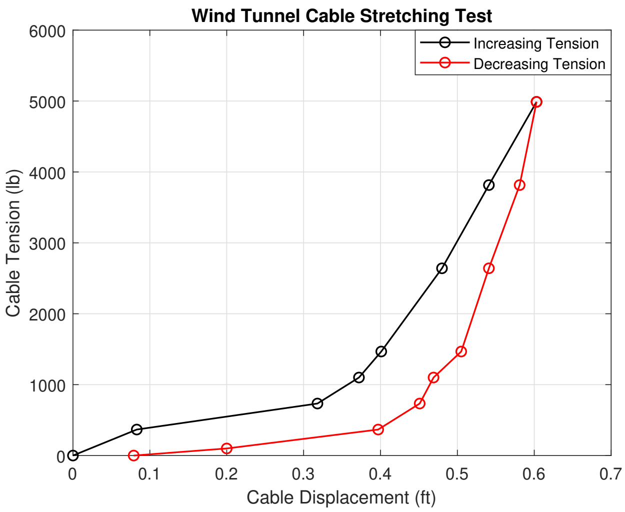

Figure 10: Wind tunnel cable stretching property

Another dynamic inconsistency between the simulation and the test was the suspension model. To measure the sling characteristic, a test procedure was developed for loading and unloading the sling used in the tunnel. The procedure was conducted in a quasi-static manner and did not capture any dynamic effects during the loading/unloading process. Figure 10 shows the result from the stretching test where strong nonlinearity between the force and displacement was present. The mismatch between the curves for increasing and decreasing tension indicated hysteretic behavior of the test cable. The ideal modeling approach would be to construct an analytical model that duplicates the hysteretic cable system such as a Bouc-Wen model ([12],[13]). However, due to the lack of cable displacement rate from the test data, it was chosen to model the nonlinearity of the cable by implementing the averaged curve of the two as a look-up table. It was found that this approach produced satisfactory consistency between the simulation and the test.

4.2. Comparison between simulation and wind tunnel result

With the addition of unsteady aerodynamics and nonlinear cable elasticity to the simulation model, the model was compared with the test results at several test speeds.

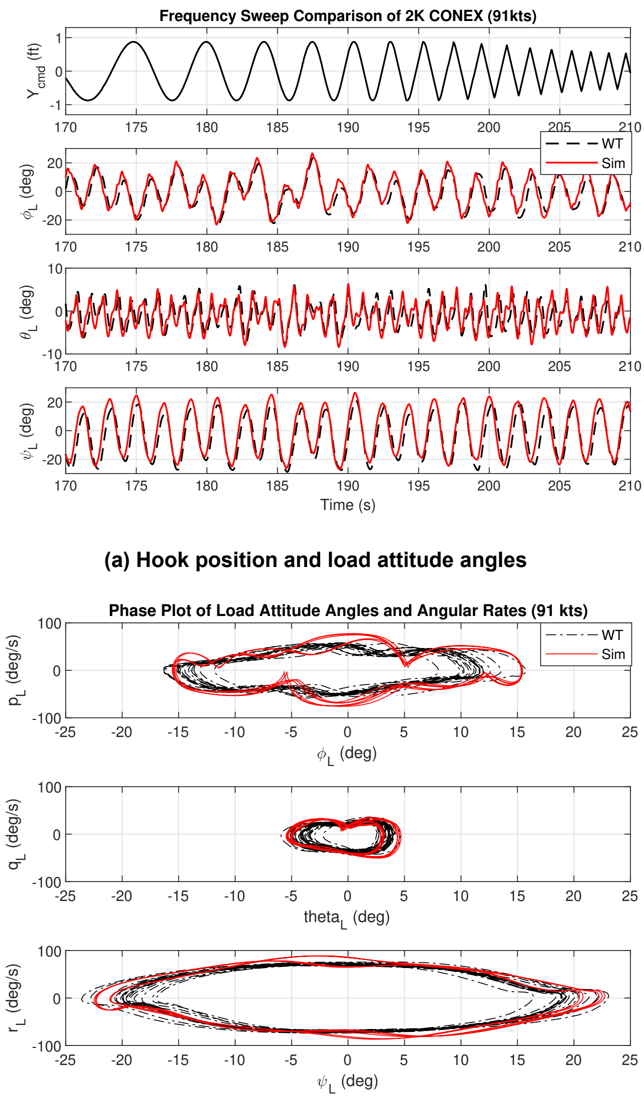

(a) Hook position and load attitude angles

(b) Phase plot of load attitude angles and angular rates

Figure 11: Frequency sweep comparison between Sim and WT (91 kts)

The frequency sweep input from the test was duplicated in the simulation and the load responses were compared with the test results. Figure 11 shows the comparison of the load attitude angles for the test speed of 91 knots. In figure 11(a), the simulation results showed very good agreement with the test results on all three axes. Figure 11(b) shows the phase plot of the three axes with angular rates and attitude angles, and it shows that the simulation had good matching of the load oscillation amplitudes, especially in roll and yaw. Figure 12 shows the time histories of the hook force direction angles and hook force magnitudes within a 10-second window. The lateral angles ϕ_F, ϕ_R showed good agreement of the oscillation around the LCO frequency with the simulation result having a smaller amplitude compared to the test results. The longitudinal angles θ_F, θ_R matched the general trend but had discrepancies in the steady-state value. The hook force magnitudes τ_F, τ_R show that the simulation predicted higher force magnitude, especially in the rear hook where the peak was around twice as large as the test curve.

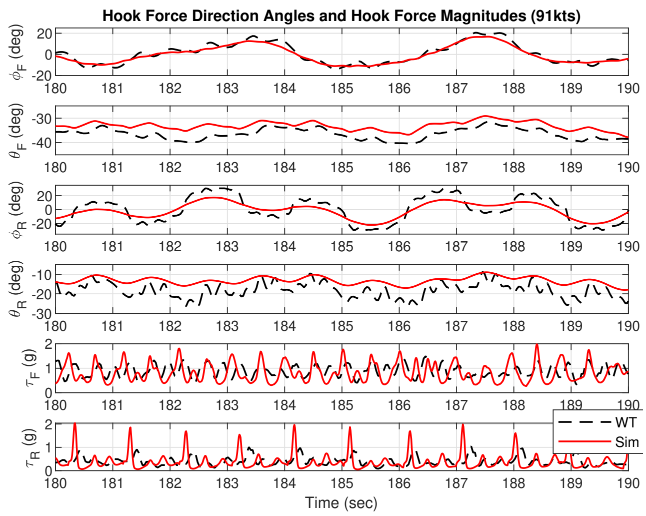

Figure 12: Hook force direction angles and hook force magnitudes (91 knots)

Figure 13 shows the bode plots of the frequency response of the load roll (ϕ_L) and yaw (ψ_L) attitudes to the lateral hook (Y_{cmd}) excitation. The first two plots of figure 13(a) show that the simulation model captured the low-frequency lateral pendulum mode and the roll-yaw-coupled mode very well in both magnitude and phase. The third plot shows the coherence function. The coherence function indicates how well the system is characterized as a linear process across the frequency range. The coherence at the lateral pendulum mode (around 1.4 rad/s) is well above 0.6, which suggests good accuracy at the corresponding frequency. The coherence drops around the roll-yaw-coupled mode which indicates that the linear correlation between the mode and the input is weak. At higher frequencies, noise becomes dominant and it is hard to distinguish the higher-order stretching mode above 10 rad/s. Figure 13(b) shows the frequency response of the load yaw attitude to the lateral hook. The responses from both the test and simulation model show the magnitude peak and phase drop around the roll-yaw-coupled mode and have good agreement with each other.

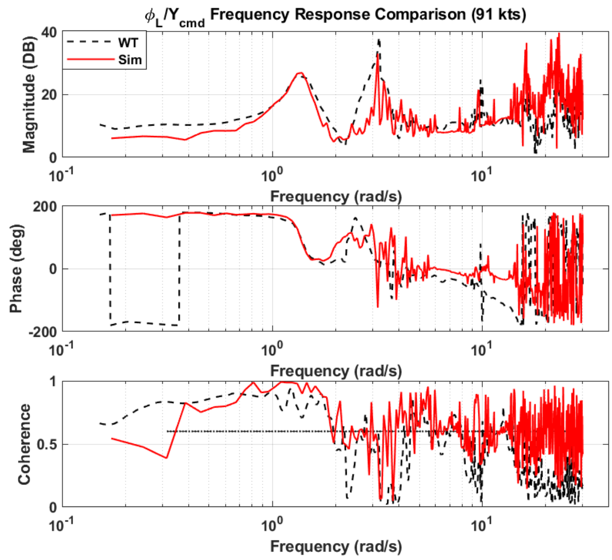

(a) Frequency response comparison of ϕ_L/Y_{cmd} (91 knots)

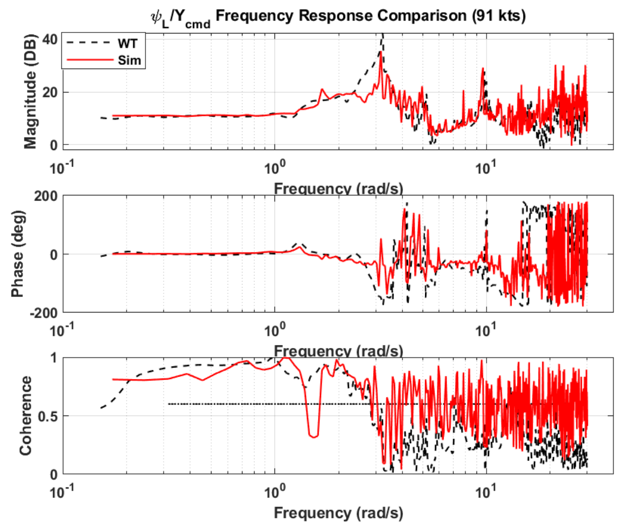

(b) Frequency response comparison of ψ_L/Y_{cmd} (91 knots)

Figure 13: Frequency response comparison between Sim and WT (91 kts)

From the comparison in both time and frequency domains, we can see that the simulation model predicted the load dynamics well and captured the unstable lateral-directional dynamics in forward flight. However, the high-frequency cable stretching mode seen in the wind tunnel test was not present in the time response of the simulation data. This suggested that the suspension model in the simulation did not replicate the test set-up completely although it did not affect the simulation of the unstable load modes. The next step was to look at the linear analysis of the model and study the change in load dynamics across the speed envelope.

4.3. Linear analysis

Linear analysis was performed for the full-size 2K load model and showed 6 oscillatory modes derived from the 12 rigid body states. Table 2 shows the eigenvalues of the 6 rigid body modes of the load at a sample speed of 91 knots with two unstable modes: the lateral pendulum mode and the roll-yaw-coupled mode.

Airspeed 91 knot
Lateral cable stretching: $-1.25+/-19.9i$
Longitudinal cable stretching: $-0.677+/-18.4i$
2^{nd} Longitudinal cable stretching: $-1.49+/-9.88i$
Roll-yaw-coupled: $0.342+/-4.40i$
Longitudinal pendulum: $-0.062+/-2.04i$
Lateral pendulum: $0.003+/-1.32i$

Table 2: Eigenvalues of dynamic modes (91 knots)

The system modes can be categorized based on the composition of the eigenvectors associated with each mode's eigenvalues. Individual elements of each eigenvector were first normalized to eliminate the effect of different units. There were 20 elements in each eigenvector including 12 rigid body states, 4 hook force direction angles, and 4 cable tensions. For the twelve rigid body states, the Euler angles (ϕ_L, θ_L, ψ_L rad) were normalized by 1, the angular rates (p_L, q_L, r_L rad/s) were normalized by the effective simple pendulum frequency defined by $\sqrt{\frac{g}{l_{c.g.}}}$, where $l_{c.g.}$ was defined as the length from the midpoint between the hooks to the load c.g. position, the velocities (u_L, v_L, w_L ft/s) were normalized by the term $\sqrt{\frac{g}{l_{c.g}}} \cdot l_{c.g.}$, and the positions ($x_E, y_E, z_E$ ft) were normalized by $l_{c.g.}$. The hook force directions angles were normalized by 1. Tensions of the four cables were added to the eigenvectors to reveal the participation of cable stretching in each mode, and they were normalized by the load weight. Individual elements of the normalized eigenvector were then weighted with respect to the absolute sum of the eigenvector. This provided the weights of each state and along with the phase information, the nature of the mode could be better understood.

Figure 14 shows the eigenvector plot of the load lateral pendulum mode and roll-yaw-coupled mode. The length of each arrow was normalized with respect to the element that had the largest weight. The states that were not plotted had minimal effects on the mode. The match in phase between the load roll attitude and

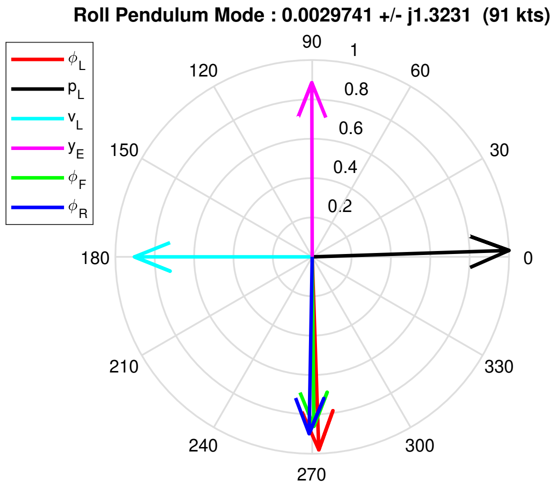

(a) Eigenvector plot of load lateral pendulum mode

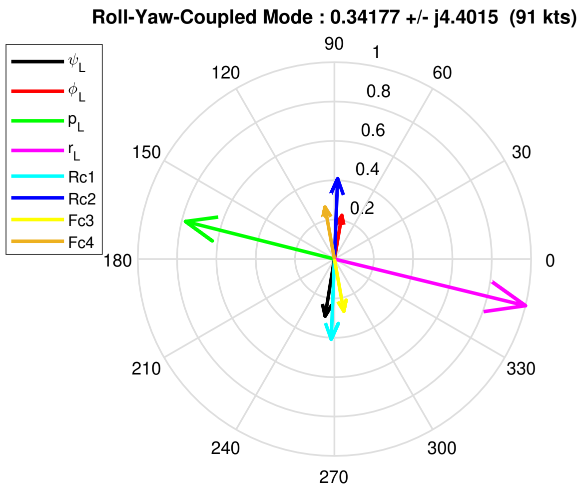

(b) Eigenvector plot of load roll-yaw-coupled mode

Figure 14: Eigenvectors of load dynamic modes (91 knots)

the lateral hook force direction angles indicated a pendulum nature in the lateral direction. All 6 states had a similar magnitude which indicated the mode response was equally distributed to all the states. The second plot includes the rear cable tensions (Rc1, Rc2) and the forward cable tensions (Fc3, Fc4) as they were largely coupled to the roll-yaw dynamic mode. The diagonal cables were in phase (Rc1/Fc3, Rc2/Fc4) and had a phase difference of 180°between the two pairs. This explains that the yawing rotation of the load caused the tensions of one pair of diagonal cables to increase and the other pair to decrease or collapse. Hence the cable stretching property had a strong effect on the characteristic of the mode.

Figure 15 shows the eigenvalues of the linearized load model across the speed envelope from 0-200 knots.

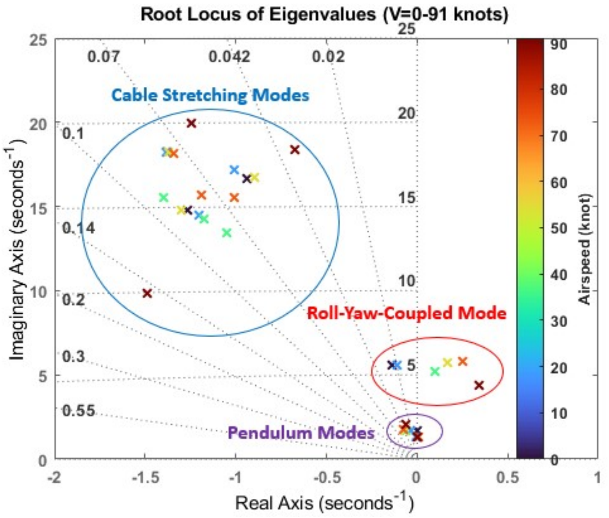

(a) V=0-91 knots (before rear cables collapse)

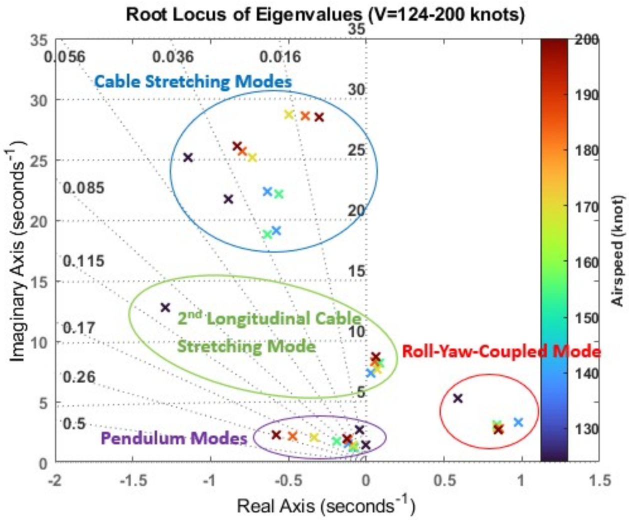

(b) V=124-200 knots (after rear cables collapse)

Figure 15: Eigenvalues of load dynamic modes

The first plot shows the eigenvalues for the airspeed range before the rear cable became slack at around 105 knots. At airspeeds below 50 knots, the load was stable with lightly-damped pendulum modes in the lateral and longitudinal axes. The lateral pendulum mode and the roll-yaw-coupled mode became unstable at speeds above 50 knots, which matched the result from the wind tunnel airspeed sweep. At airspeeds above 105 knots, an unstable mode around 7-9 rad/s appeared which was associated with the 2^{nd} longitudinal cable stretching mode. The unstable roll-yaw-coupled mode was still present located further to the right in the real axis. The unstable pendulum mode became stable and remained lightly damped.

5. CONTROL DESIGN

After validating the accuracy of the simulation model, an active hook controller was designed to improve the stability of the load across a wider airspeed range. The control design used similar design methods as presented in [7] for a single-point load.

5.1. Initial Tests

As an initial test, the controller from [7] was applied directly in the wind tunnel test of the dual-point suspended 2K CONEX. The ACH used cable angle (same as hook force direction angles) feedback to drive the lateral position of the forward hook position using a lagged cable angle feedback compensator. Surprisingly, the controller showed stabilizing effect on the unstable CONEX in a limited speed range, even though the load tested in [7] (an M119 howitzer) was completely different from the CONEX.

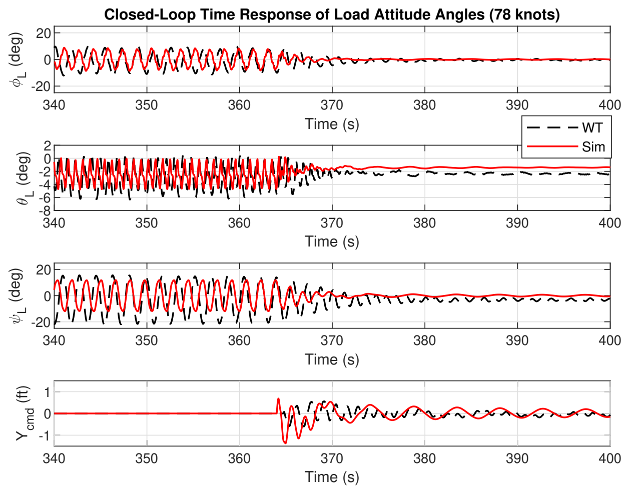

Figure 16: Comparison of closed-loop responses with wind tunnel test controller (78 knots)

The same controller was tested for the simulated 2K CONEX load. It was found that the controller was able to stabilize the simulated load when using the load roll attitude angle as feedback. Figure 16 shows the closed-loop time histories of the load attitude angles from the test result and simulation with the test controller. It shows that after the controller was turned on at 364 seconds, the load LCO was quickly damped out in both environments. However, it was found that the simulated load was not stabilized by the test controller when using cable angle feedback (as was used in the test). This discrepancy is not yet fully understood and warrants further investigation.

5.2. Lagged roll angle feedback controller

The next step was to design a controller based on the true dynamics of the 2K CONEX with dual-point suspension. The linearized dynamics extracted from the simulation model (as described in the previous section) were used to design a lagged roll angle feedback control law using classical methods, as was first presented in [14] and later applied in [7].

$$\frac{Y_{cmd}}{\Delta\phi_L} = \frac{K\omega^2 s}{(s+0.1)(s^2+2\zeta\omega s+\omega^2)} \tag{6}$$

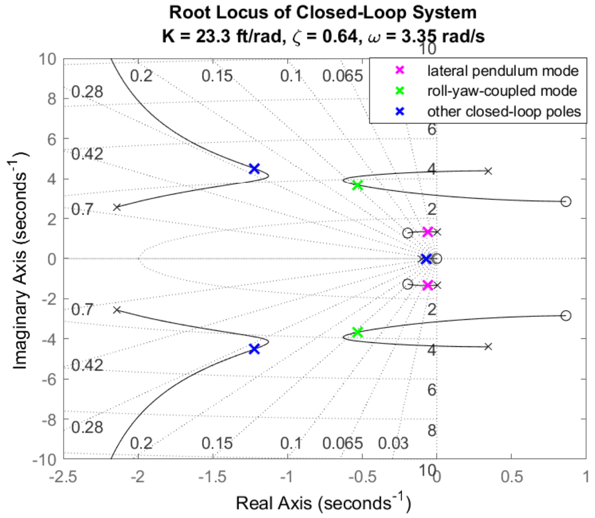

Figure 17: Root locus plot of the closed-loop system with load roll angle feedback (91 knots)

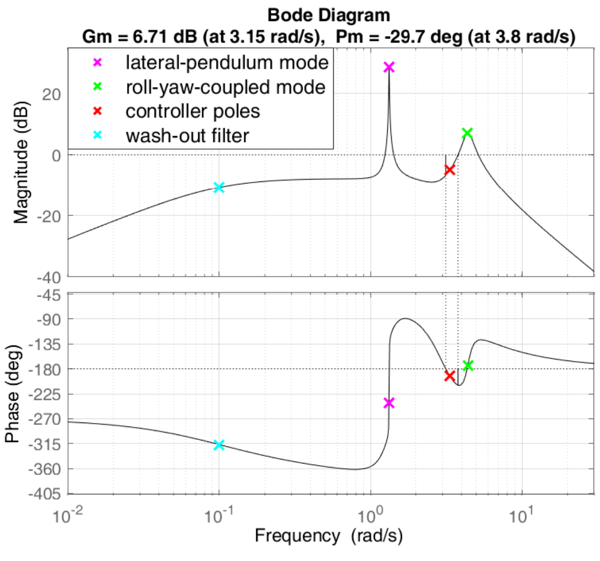

Figure 18: Bode Diagram of the closed-loop system with load roll angle feedback (91 knots)

For airspeeds below 110 knots, a linear controller was designed using lagged load roll angle feedback to stabilize the unstable lateral-directional modes of the system. The linear controller is shown in equation 6. It is comprised of a wash-out filter for rejecting steady-state input with a wash-out frequency of 0.1 rad/s, and a 2^{nd} order denominator that introduces phase lag at a specified frequency. The K parameter is the feedback gain.

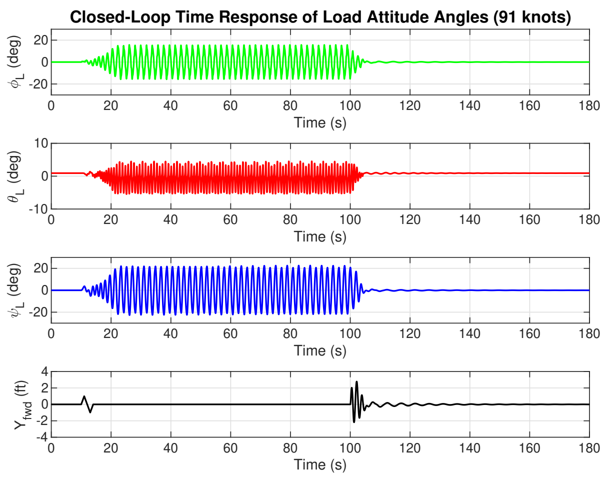

Figure 19: Time response of the closed-loop system with load roll angle feedback (91 knots)

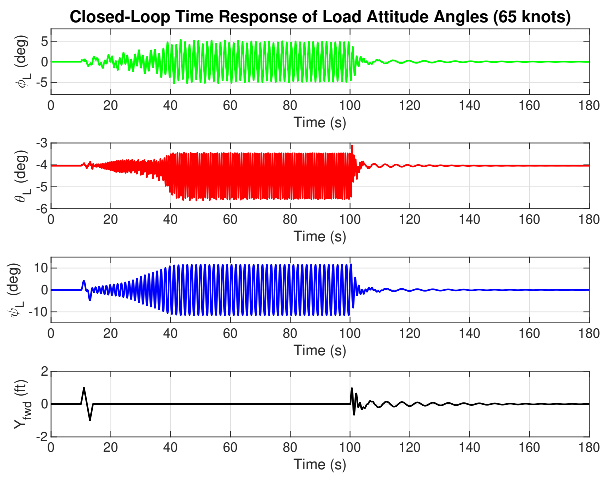

Figure 20: Time response of the closed-loop system with load roll angle feedback (65 knots)

Figures 17 and 18 show the root locus plot and bode diagram for the sample airspeed of 91 knots. With a selection of controller parameters listed in figure 17 ($K = 23.3 ft/rad, \zeta = 0.64, \omega = 3.35 rad/s$), the closed-loop poles of the system were stabilized. The natural frequency of the 2^{nd} order denominator from the controller was placed in between the lateral pendulum mode frequency and the roll-yaw-coupled mode frequency. From the second plot in figure 18, it shows that the 2^{nd} order denominator introduced phase reduction over the frequency range between the two unstable modes. Essentially, it introduces phase lag so that the phase is below -180°at the gain crossover frequency. This resulted in a stable closed-loop system with a gain margin equal to 6.71 dB and a phase margin equal to -29.7 degrees. The negative phase margin represents the maximum

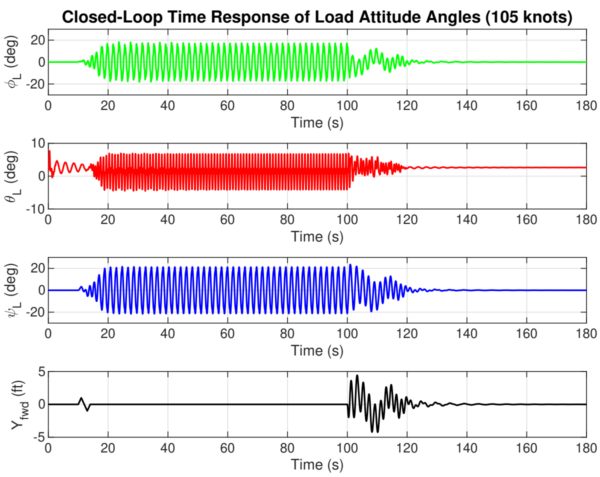

Figure 21: Time response of the closed-loop system with load roll angle feedback (105 knots)

amount of allowable phase lead that can be added to the system before it becomes unstable. The gain parameter K was chosen such that the gain margin and phase margin were maximized for robustness. However, it is observed that the damping ratios of the closed-loop poles are small, especially with the lateral pendulum mode which has a damping ratio below 0.1. The cause of this can be due to the complex dynamics of the dual-point CONEX and the limited authority of the forward active hook on load stabilization in forward flight.

The designed linear controller was integrated into the nonlinear simulation model for performance validation. The model was simulated at the design airspeed (figure 19) and several other airspeeds (figures 20-21), and the closed-loop time response showed that the controller was able to stabilize the load at different airspeeds without adjustment on the controller parameters. Although it was expected that a gain-scheduled controller will achieve better performance than a universal controller.

5.3. Cable length adjustment controller

From both wind tunnel tests and simulation, it was found that the load distributions between the forward and rear hooks differed drastically during highspeed flights. The forward hook force increased with airspeed and the rear hook force decreased. Eventually, the cables connecting the load and the rear hook became slack. This is concerning as the high forward hook force could cause safety issues, which prevents the load from being carried at a higher airspeed. A controller was designed that can automatically adjust the length of the rear cables to alleviate the load in the front by reducing the rear cable length. This also provides authority to the forward hook for active stabilization at higher airspeeds. Figure 22 shows the block diagram for the cable length adjustment controller. The reference cable length was 16 ft for both forward and rear cables. The cable force dynamics were approximated with a gain value K, which was implemented as a look-up table in the nonlinear simulation model, and multiplied with a low-pass filter to eliminate high-frequency signals. While this was not an exact representation of the cable force dynamics, it served the purpose of providing a linear model for controller design. The value of the ratio K_I/K_P was selected to be small to achieve a slow and steady action when adjusting the cable length so that it would not introduce any instability to the load.

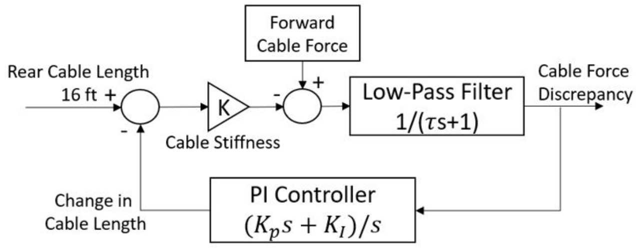

Figure 22: Block diagram of the cable length adjustment controller ($\tau = 10sec, K_P = 0.001, K_I = 0.0005$)

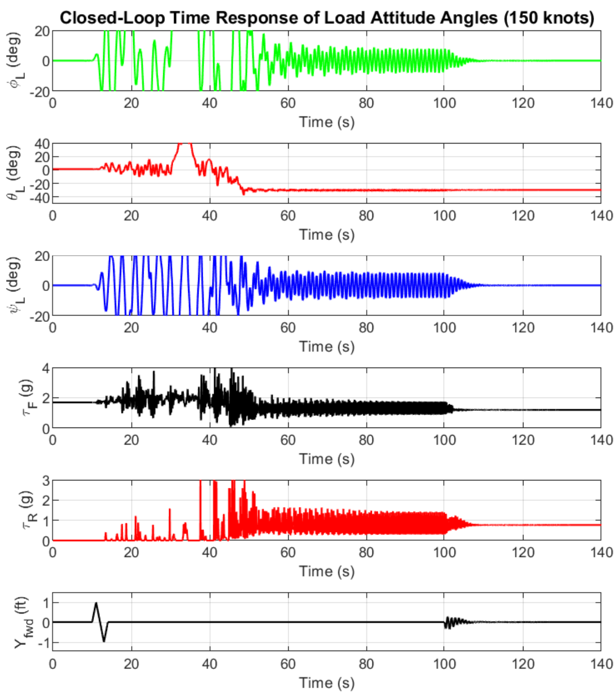

Figure 23: Time response of the closed-loop system with cable length adjustment and ACH controllers

The designed cable length adjustment controller was simulated at higher airspeed where the rear cable was slack. Figure 23 shows the time response of the closed-loop system simulated at 150 knots. Without any control action, the load displayed chaotic oscillations in all axes. The rear cable was slack as reflected by the rear hook force magnitude curve. The cable length adjustment controller was turned on at 40 seconds, which quickly reduced the oscillation amplitude of the load in the lateral-directional axes and brought the rear hook force magnitude closer to the forward hook force magnitude. The ACH controller with a slightly raised natural frequency of the 2^{nd} order denominator was turned on at 100 seconds. As a result, it further damped out the oscillations and stabilized the load with minimal hook usage.

6. CONCLUSIONS

Summary:

1. The dynamic characteristics of a dual-point CONEX load model were studied in wind tunnel tests and simulations. The wind tunnel test has revealed the unstable nature of the roll-yaw degrees of freedom above 50 knots full-scale and demonstrated the ability of a lateral ACH on the forward hook to stabilize the load. The simulation model of the full-scale configuration showed good agreement with the wind tunnel test results over the airspeed range tested in the tunnel. The simulation model extends the speed envelope for analyzing load dynamics beyond what could be tested in the tunnel.
2. ACH control design was conducted for the CONEX load and it showed successful load stabilization using load attitude angle feedback at airspeeds below 110 knots.
3. A cable length adjustment controller was designed to alleviate forward hook force during highspeed flights and showed stabilizing effect on the load LCO motion.
4. Although it was expected that dual point carriage may help in solving problems associated with a single-point load, it introduces new problems such as LCO at relatively low speeds and rear cables becoming slack at higher speeds. Years of research on single point carriage led to the ability to develop good simulation tools that had shown very good agreement with test results. It seems that research efforts are still needed in order to develop a dual-point simulation of the same quality. As in the case of a single-point carrier, it seems that the most efficient method of coping with problems of dual-point carriage will include simulation tools, wind tunnel tests, and flight tests.

7. ACKNOWLEDGMENTS

This research was carried out in cooperation with US Army DEVCOM AvMC under the US-Israel Rotorcraft Project Agreement for cooperative research. The research at Penn State was partially funded by the US government under Agreement No W911W6-17-2-0003.

8. REFERENCES

[1] R. W. Gabel and G. J. Wilson. "Test Approaches to External Sling Load Instabilities". In: *Journal of the American Helicopter Society* 13.3 (1968), pp. 44–55.

[2] D. F. Pryor and J. Sheldon. *A Study In Depth of A Single Point and Two Point Lateral and Tandem Suspension of Rectangular Box Loads*. Tech. rep. AM/38. Royal Military College of Science Department of Mechanical Engineering, Apr. 1973.

[3] D. G. Miller, Y. Lu, F. White, E. M. Osciak, B. Robert, R. Price, and J. Wiedorn. "Flight Simulation as a Tool to Develop V-22 Slung Load Capabilities". In: *55th Annual Forum of the American Helicopter Society*. 1999.

[4] H. J. Sommer III, J. M. Cimbala, and D. G. Miller. "Self-Excited Limit Cycle Yaw Oscillation Instability of External Sling Payloads with Dual-Point Suspension During Level Flight". In: *Journal of the American Helicopter Society* 60.4 (2015), pp. 1–10.

[5] L. S. Cicolani, J. G. A. da Silva, E.P.N Duque, and M. B. Tischler. *Unsteady Aerodynamic Model of a Cargo Container for Slung-Load Simulation: Preliminary Aerodynamic Data and Model Identification*. Tech. rep. TP-2004-212817. NASA, May 2004.

[6] R. Raz, A. Rosen, J. Lusardi, L. Cicolani, and W. Robinson. "Wind Tunnel and Flight Evaluation of Stability and Passive Stabilization of a Cargo Container Slung Load". In: *64th Annual Forum of the American Helicopter Society*. Apr. 2008.

[7] R. Raz, A. Rosen, S. J. Nadell, L. S. Cicolani, J. F. Horn, J. Enciu, Z. Chen, M. B. Tischler, and K. K. Cheung. "Hardware-in-the-Loop Dynamics Wind Tunnel Investigation of Slung Loads Dynamics with Application to Active Cargo Hook Stabilization of an M119 Howitzer". In: *76th Annual Forum of the American Helicopter Society*. Oct. 2020.

[8] L. S. Cicolani, J. Lusardi, L. D. Greaves, D. Robinson, A. Rosen, and R. Raz. *Flight Test Results for the Motions and Aerodynamics of a Cargo Container and a Cylindrical Slung Load*. Tech. rep. TP-2010-216380. NASA, Apr. 2010.

[9] A. Rosen, S. Cecutta, and R. Yaffe. *Wind Tunnel Tests of Cube and CONEX Models*. Tech. rep. TAE 844. Technion Israel Institute of Technology, Dept of Aerospace Engineering, Nov. 1999.

[10] D. Chan, J. W. Flower, and A. Simpson. *Aerodynamically Induced Motions of Bluff Bodies Suspended Beneath Helicopters*. Tech. rep. Bristol University Department of Aeronautical Engineering, Oct. 1975.

[11] A. Simpson and J. W. Flower. "Unsteady Aerodynamics of Oscillating Containers and Application to the Problem of Dynamic Stability of Helicopter Underslung Loads". In: *AGARD Conference Proceedings* 235.3 (May 1978), (13)1–33.

[12] A. G. Chassiakos, S. F. Masari, A. W. Smyth, and T. K. Caughey. "On-line Identification of Hysteretic Systems". In: *Journal of Applied Mechanics* 65 (Mar. 1998), pp. 194–203.

[13] R. Leenen. *The Modeling and Identification of an Hysteretic System: the Wire as a Nonlinear Shock Vibration Isolator*. Tech. rep. Eindhoven University of Technology, Jan. 2002.

[14] J. Krishnamurthi and J.F. Horn. "Helicopter Slung Load Control Using Lagged Cable Angle Feedback". In: *Journal of the American Helicopter Society* 60 (Apr. 2015), pp. 1–12.